



# CHORUS

This is the accepted manuscript made available via CHORUS. The article has been published as:

## Mitigation of turbophoresis in particle-laden turbulent channel flows by using incident electric fields

M. Di Renzo, P. L. Johnson, M. Bassenne, L. Villafañe, and J. Urzay

Phys. Rev. Fluids **4**, 124303 — Published 6 December 2019

DOI: [10.1103/PhysRevFluids.4.124303](https://doi.org/10.1103/PhysRevFluids.4.124303)

# Mitigation of turbophoresis in particle-laden turbulent channel flows by using incident electric fields

M. Di Renzo, P. L. Johnson, M. Bassenne, L. Villafañe, and J. Urzay  
*Center for Turbulence Research, Stanford University, Stanford, CA 94305, USA*

(Dated: November 20, 2019)

It is known that the dynamics of particles dispersed in turbulent flows can be significantly altered by electric charges and external electric fields. The next step therefore involves the investigation of whether these electric interactions can be exploited in engineering applications to control processes involving the transport of particles in turbulence. In this study, direct numerical simulations of incompressible turbulent channel flows laden with a positively iso-charged suspension of monodisperse small inertial particles are employed to investigate the effect of electric charges carried by the particles on their dispersion, and to illustrate the intentional abatement of turbophoretic effects using incident electric fields. An Eulerian/Lagrangian formulation is employed along with a fast multipole method for the electric potential conveniently corrected with wall boundary conditions. Operating conditions are identified in terms of characteristic dimensionless parameters where an AC electric field applied across the channel walls decreases the time-averaged concentration of particles near the walls by up to two orders of magnitude.

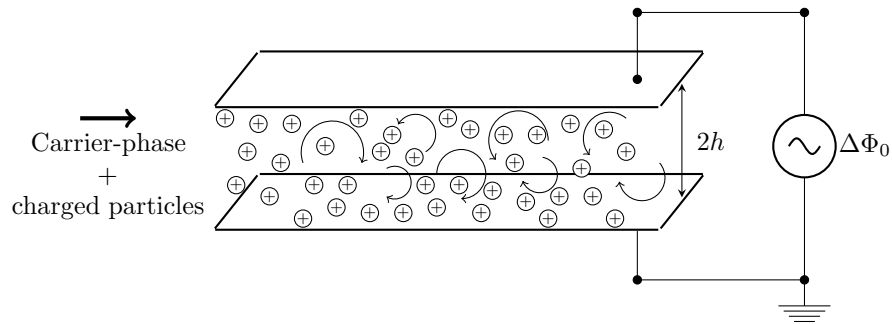


FIG. 1. Schematics of the model problem: A positively iso-charged suspension of monodisperse small inertial particles laden in a biperiodic turbulent channel flow whose walls are connected to an AC voltage source.

## I. INTRODUCTION

Wall-bounded turbulent flows laden with inertial particles are central to a number of technologically relevant physical processes. The specific form of the spatial dependence of the root-mean square (rms) of the wall-normal velocity makes wall-bounded particle-laden turbulent flows prone to develop a ponderomotive effect known as turbophoresis, whereby the particles tend to drift toward the wall and accumulate there [1, 2]. The increase of near wall particle concentration due to turbophoresis can be a desirable or deleterious effect depending on the practical application under consideration. Well-studied effects such as wall roughness [3] have been shown to reduce the accumulation of particles near the wall by altering the underlying turbulent flow. The modulation of turbophoresis by using incident electric fields is a relatively unexplored aspect that represents the focus of the present study.

In practical scenarios, the particles tend to acquire a net electric charge during their motion as they collide with each other and with the walls. Upon collision, electric-charge exchanges occur with intensities that depend on the size and material properties of the colliding objects and on the local electric field [4–8]. As a consequence, a self-induced electric field is generated by the net charge acquired by the particles, which can lead to significant modifications of their spatial distribution in the flow field [9–13]. The collective effect resulting from these electric interactions is by no means trivial to characterize as it is engendered by the integration of an  $N$ -body problem corresponding to each of the  $N$  charged particles interacting with one another and with the background turbulent flow. In isotropic turbulence, for instance, these interactions occur in such a way that the ensuing electric field is a relatively strong one that can have a strikingly large energy content at low wavenumbers [14].

In the present study, the aforementioned interactions are studied using direct numerical simulations (DNS) of a turbulent channel flow laden with positively charged, monodispersed small inertial particles. The top and bottom walls of the channel are connected to the terminals of an AC voltage source, as sketched in Fig. 1. The objective of this investigation is to quantify the effects of self-induced and incident electric fields on the spatial distribution of particles near the wall. The results suggest that a significant abatement of turbophoresis occurs under incident electric fields in particular operating conditions that are identified below in terms of characteristic dimensionless parameters.

The remainder of this paper is structured as follows. A description of the conservation equations and computational setup is provided in Sec. II. Results pertaining to two sets of cases are considered in Sec. III. In the first set of cases, which are studied in Sec. III.1, the voltage across the channel walls is set to zero, in such a way that only the electric field induced by the particle charges is at play in the solution. In the second set of cases, which are studied in Sec. III.2, the AC voltage source is switched on, and the particles are therefore subjected to an oscillating electric field across the channel walls. Lastly, a short example that translates the dimensionless results into dimensional ones are provided in Sec. IV along with concluding remarks.

## II. FORMULATION AND COMPUTATIONAL SETUP

The approach employed here is based on an Eulerian/Lagrangian formulation augmented with appropriate equations for the electric field and electric forces on the particles, as described below.

## II.1. Conservation equations

In this study, the mass and momentum conservation equations

$$\nabla \cdot \mathbf{v} = 0, \quad \rho \frac{\partial \mathbf{v}}{\partial t} + \rho \mathbf{v} \cdot \nabla \mathbf{v} = -\nabla \Pi + \mu \nabla^2 \mathbf{v} + A \mathbf{e}_x, \quad (1)$$

are integrated numerically for the carrier phase, where  $\mathbf{v}$  is the velocity vector,  $\rho$  is the density,  $\mu$  is the dynamic viscosity,  $\Pi$  is the hydrodynamic pressure, and  $A$  is a constant and uniform favorable pressure gradient externally imposed to drive the flow. The friction Reynolds number is  $Re_\tau = u_\tau h / \nu = 150$ , where  $\nu = \mu / \rho$  is the kinematic viscosity,  $h$  is equal to half of the channel height,  $u_\tau = \sqrt{\tau_w / \rho}$  is the friction velocity, and  $\tau_w = Ah$  is the wall shear stress, thereby leading to a bulk Reynolds number  $Re_b = U_b h / \nu \simeq 2100$  based on the bulk velocity  $U_b$ . The conservation equations in (1) are subject to periodic boundary conditions in the spanwise and streamwise directions, and to non-slip boundary conditions on the walls. Note that the computational setup of the unelectrified version of this configuration follows the benchmark simulations of Marchioli *et al.* [15]. The basic observations made in this paper, scaled in inner units, are expected to hold for higher Reynolds numbers.

The formulation of the dispersed phase is based on a Lagrangian description given by

$$\frac{d\mathbf{x}_p}{dt} = \mathbf{v}_p, \quad \text{and} \quad \frac{4}{3}\pi\rho_p a_p^3 \frac{d\mathbf{v}_p}{dt} = 6\pi\mu a_p (\mathbf{v} - \mathbf{v}_p) + \mathbf{F}_p, \quad p = 1, \dots, N, \quad (2)$$

which represent, respectively, the trajectory equation and the second Newton's law for every particle. In this formulation,  $\mathbf{x}_p$  and  $\mathbf{v}_p$  are, respectively, the position and velocity of the  $p$ -th particle. Similarly,  $\rho_p$  and  $a_p$  denote, respectively, the density and radius of the particles, these two quantities being the same for all particles in this study. Implicit assumptions involved in writing the drag force in the second equation in (2) are: (a) that the density ratio  $\rho_p / \rho \gg 1$  is large; (b) that the characteristic Reynolds number of the particles based on the relative velocity  $Re_p = |\mathbf{v} - \mathbf{v}_p| a_p / \nu \ll 1$  is small; (c) that the gravitational acceleration  $g$  is negligible compared to the characteristic particle acceleration  $u_\tau / t_a$ , where  $t_a = (2/9)(\rho_p / \rho) a_p^2 / \nu$  is the characteristic acceleration time of the particles; and (d) that the particles are much smaller than all hydrodynamic scales,  $a_p / \delta_\nu \ll 1$ , where  $\delta_\nu = \nu / u_\tau$  is the thickness of the viscous sublayer. In this small particle limit, the lift force on particles becomes small, so is neglected at present. However, the role of the lift force [16–18] is a topic of interest for future investigations of scenarios similar to those considered here.

A total number of  $N = 10^5$  particles are employed in the simulations, thereby leading to a sufficiently small value of the mean mass-loading ratio  $\alpha = (4/3)\pi\rho_p n_0 a^3 / \rho \ll 1$  that enables one-way coupling with the carrier phase, with  $n_0 = N / (16\pi^2 h^3)$  being the mean number density of particles. The particles are assumed to collide elastically against the channel walls and among each other. In particular, collisions between particles, which have an important effect on turbophoresis even at relatively small volume fractions [19–22], are computed using the hard-sphere collision model. While the collision model is simplified for the present purposes, the impact of more detailed collision models may be of interest for further study on this topic.

In Eq. (2), the  $\mathbf{F}_p = q_p \mathbf{E}_p$  denotes the net electric force on the  $p$ -th particle, where  $q_p$  is the particle charge, which is assumed to be positive and equal for all particles, and  $\mathbf{E}_p = \mathbf{E}_p^\infty + \mathbf{E}_p^w$  is an electric field obtained from the superposition of two components. The first component  $\mathbf{E}_p^\infty$  is the Coulombic field generated by the cloud of  $N - 1$  particles surrounding the  $p$ -th particle located at position  $\mathbf{x}_p$  in an unbounded domain, namely  $\mathbf{E}_p^\infty = -\nabla \phi^\infty|_{\mathbf{x}=\mathbf{x}_p} = (4\pi\epsilon_0)^{-1} \sum_{j=1, j \neq p}^N q_j (\mathbf{x}_j - \mathbf{x}_p) / (|\mathbf{x}_j - \mathbf{x}_p|^3)$  where  $\phi^\infty$  is the corresponding electrostatic potential and  $\epsilon_0$  is the vacuum permittivity. The second component  $\mathbf{E}_p^w$  is a correction that serves to impose appropriate boundary at the walls, and is obtained by integrating the Gauss law  $\nabla^2 \phi^w = 0$  in the computational domain, where  $\phi^w$  is the corresponding correction for the electrostatic potential defined by the relation  $\mathbf{E}_p^w = -\nabla \phi_p^w|_{\mathbf{x}=\mathbf{x}_p}$ . The Gauss law for  $\phi^w$  is integrated subject to periodic boundary conditions in the streamwise and spanwise directions, and to a set of specific boundary conditions that lead to iso-potential walls proper to electrically conducting materials. In particular, the boundary condition  $\phi^w = -\phi^\infty$  is applied on the bottom wall to keep it grounded at all times. The boundary condition  $\phi^w = \Delta\Phi - \phi^\infty$  is applied on the top wall, which enforces an oscillating voltage difference  $\Delta\Phi = |\Delta\Phi_0| \cos(\omega_{el} t)$  between the two walls with amplitude  $|\Delta\Phi_0|$  and angular frequency  $\omega_{el}$ .

It is worth mentioning that the integration of (2) incurs an unfeasible computational cost of order  $N^2$  per time step if all particles were simultaneously considered. An alternative approach that decreases the computational cost to order  $N \log N$ , while keeping a relatively high level of fidelity in the calculations, is the fast multipole method (FMM) originally proposed in [23] and recently employed in [14] to describe the dynamics of electrified particles in homogeneous-isotropic turbulence. Specifically, the FMM computes exactly the contribution to the electric field of

the particles that are near the  $p$ -th particle. However, the effects of particles classified as being far away according to an octree algorithm are approximated using a tenth-order accurate Laplace expansion of the electrostatic potential [i.e., see [14] for details].

In this study, charge transfer upon collisions is neglected because of the small volume fractions of order  $10^{-6}$  involved in the simulations. Similarly, all particles are assumed to have positive and equal charge. This case is illustrative of the long-time charge state in a turbulent channel flow laden with monodisperse particles, when particles have had sufficient time to collide against the walls, acquire their charge signs, and redistribute the charge among other particles through collisions.

## II.2. Characteristic dimensionless parameters

Besides  $Re_\tau$ , additional important dimensionless parameters participate in the solutions that are worth discussing. Relative inertial effects are measured by the following three Stokes numbers: (a) the aerodynamic Stokes number  $St_{ae}^+ = t_a/t_\nu$ , where  $t_\nu = \delta_\nu^2/\nu$  is the viscous time scale; (b) the internal electric Stokes number  $St_{el}^{int} = u_{el}^{int}/u_\tau$ , which corresponds to the ratio of the characteristic wall-normal electromigration velocity  $u_{el}^{int} = n_0\delta_\nu q_p^2/(6\pi\mu\epsilon_0 a_p)$ , generated by the self-induced bulk electric-field scale  $E_0 = q_p n_0 \delta_\nu / \epsilon_0$ , to the friction velocity  $u_\tau$ ; and (c) the external electric Stokes number  $St_{el}^{ext} = u_{el}^{ext}/u_\tau$ , which measures the effects of the incident electric field on the particles, and is based on the characteristic wall-normal electromigration velocity  $u_{el}^{ext} = |\Delta\Phi_0|q_p/(12\pi\mu a_p h)$  produced by the incident electric-field scale  $|\Delta\Phi_0|/(2h)$ . The period of oscillation of the AC electric field relative to the flow time scales is quantified by the dimensionless frequency  $\omega_{el}^+ = \omega_{el} t_\nu$ . Lastly, the dimensionless particle radius  $a_p^+ = a_p/\delta_\nu$  determines the effective collision cross section of every point particle in the flow upon elastic collision with other particles and the wall. While  $a_p^+ = 0.17$  and  $St_{ae}^+ = 5.0$  are representative values that are kept fixed in all the cases described below, the parameters  $St_{el}^{int}$ ,  $St_{el}^{ext}$ , and  $\omega_{el}^+$  are varied over wide ranges to study their influences on the solution.

## II.3. Computational setup

The conservation Eqs. (1) are solved in a cuboidal computational domain, whose dimensions are  $4\pi h \times 2h \times 2\pi h$  in the streamwise ( $x$ ), wall-normal ( $y$ ), and spanwise ( $z$ ) directions, and which is discretized using a staggered Cartesian grid with  $192 \times 129 \times 160$  nodes. The nodes in the wall-normal direction are spatially distributed using a hyperbolic-tangent stretching corresponding to a size  $\Delta y^+ = 0.50$  of the first grid cell and a maximum wall-normal grid spacing of  $\Delta y^+ = 4.3$  at the centerline of the channel. The Kolmogorov scale at the centerline for this flow was estimated to be  $\eta^+ = 3.6$  by [15]. A grid overlaid on the mesh used to solve the flow field, consisting of 193 nodes along the wall-normal direction, and subject to hyperbolic-tangent stretching factor in the same direction corresponding to a size  $\Delta y^+ = 0.36$  of the first grid cell, is employed to construct the Eulerian number-density field  $n$ , as recommended in [15] for the same range of flow parameters studied here.

The carrier-phase conservation Eqs. (1) are integrated on a staggered Cartesian mesh with second-order central differencing. The time advancement employs a fractional step procedure for pressure projection within a second-order Runge-Kutta method [24]. The time step chosen was  $\Delta t^+ = 0.06$  to ensure accurate results. The dispersed-phase equations (2) are advanced in time with the same scheme as the flow and are supplied with trilinearly-interpolated values of the electric field  $\mathbf{E}^w$  and the carrier-phase velocity at the particle location. The Gauss equation for  $\phi^w$  is solved as part of the same computational algorithm employed for integrating the Poisson equation for the hydrodynamic pressure.

The calculations were initialized using a statistically steady-state distribution of the concentration field of uncharged particles, and the flow was integrated thereafter for  $9000t_\nu$  time units before collecting data for time averaging. Time-averaged statistics were computed by averaging 11 solution snapshots evenly distributed over a period of  $18000t_\nu$  time units. Phase-averaged statistics were calculated by collecting 800 solution snapshots evenly distributed over 20 cycles of the applied oscillating voltage.

The statistical convergence of the results was checked in the following way. The time-averaged profile of the concentration of particles in the unelectrified case was observed to remain unaltered when the number of snapshots was increased to 22 over a longer sampling time equal to  $36000t_\nu$ . Similarly, the phase-averaged spatial distribution of the concentration of particles in the electrified case corresponding to  $St_{el}^{int} = 10^{-6}$ ,  $St_{el}^{ext} = 10^{-2}$ , and  $\omega_{el}^+ = 0.002\pi$ , which represents the most unfavorable case for convergence because of the associated small value of voltage frequency,

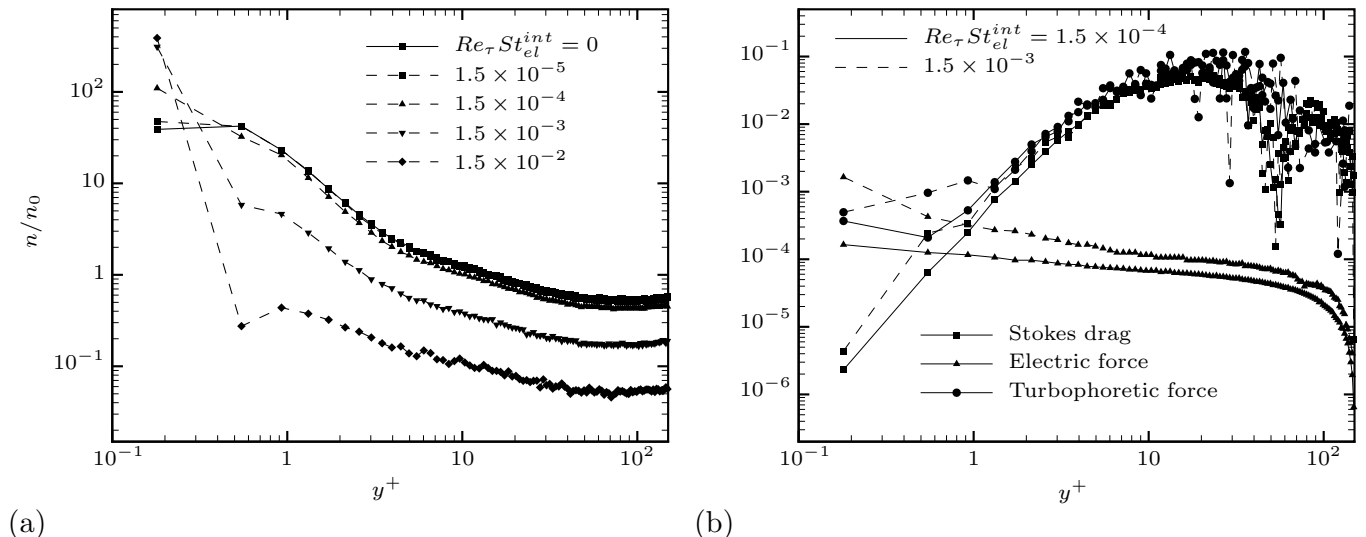


FIG. 2. Dispersed-phase statistics without an applied electric field: (a) Time-averaged number-density profiles in the wall-normal direction for increasing values of  $Re_\tau St_{el}^{int}$ , and (b) wall-normal profiles of the absolute value of each term on the right-hand side of the momentum balance Eq. (5) multiplied by  $\langle n^* \rangle^{-1}$ .

was observed to remain unaltered when the number of snapshots was increased to 1600 over a longer sampling time equivalent to 40 cycles of the applied voltage.

### III. RESULTS

This section focuses on the description of the results obtained by numerically integrating the formulation outlined above. Cases in which there is no incident electric field are described first in Sec. III.1, since the character of the internal electric field induced by the charged particles proves to be important for the discussion. The effects of external oscillating electric fields on the distribution of particles are analyzed in Sec. III.2.

#### III.1. Collective effects of self-induced electric fields

Time-averaged wall-normal profiles of number densities of particles are shown in Fig. 2(a) for cases without an incident electric field,  $|\Delta\Phi_0| = 0$  (i.e.,  $St_{el}^{ext} = 0$ ). In interpreting the results, it is important to note that, while the typical turbophoretic increase in number density is observed in the case corresponding to uncharged particles ( $St_{el}^{int} = 0$ ) as the wall is approached, the cases where particles are charged ( $St_{el}^{int} > 0$ ) are characterized by a significant transfer of particles from the bulk of the channel to a thin region close to the wall whose thickness in viscous units is of order unity. It is therefore concluded that the self-induced electric field exacerbates the tendency of the particles to accumulate near the wall, with increasingly sharper slopes of  $n$  being observed in the concentration profiles as  $St_{el}^{int}$  increases. The phenomenon described above is clearly reminiscent of the charge-relaxation mechanism that occurs in electrical conductors whereby the charges tend to drift toward the shell of the conductor, thereby leaving the core of the conductor in electroneutral conditions. In the present problem, however, the charges are not completely free to migrate since the particles are also subjected to aerodynamic forces.

In order to further investigate the effects of the self-induced electric field on the concentration profiles, it is expedient to derive a representative conservation equation for the momentum of the dispersed phase that is amenable to discussion by following the statistical approach first formulated by Williams [25] for spray droplets, and hereafter applied to charged solid particles. The analysis is facilitated by the statistically steady state and double periodicity of the flow, in that the statistics vary predominantly only in the wall-normal direction, with additional time variations being required if the effects of applied oscillating fields were included. With these approximations in mind, consider

the probable number of particles  $f(y, v_p)dydv_p$  located between  $y$  and  $y + dy$  and moving with wall-normal velocities between  $v_p$  and  $v_p + dv_p$ . In this formulation  $f$  is a distribution function that is normalized as  $\int_{-\infty}^{+\infty} \int_0^{2h} f dy dv_p = N$  and satisfies the transport equation

$$\frac{\partial}{\partial y^+}(v_p^+ f) + \frac{\partial}{\partial v_p^+} \left[ \left( \frac{\langle v^+ | y_p^+ \rangle - v_p^+}{St_{ae}^+} + \frac{St_{el}^{int}}{St_{ae}^+} \langle E_y^+ | y_p^+ \rangle \right) f \right] = Da \left( \frac{\partial f}{\partial t} \right)_{coll}^*, \quad (3)$$

where the angular bracket operator  $\langle \cdot | y_p^+ \rangle$  indicates ensemble averaging conditioned on the particle position. Additionally  $E_y^+ = E_y/E_0$  is the dimensionless wall-normal component of the electric field obtained from integration of the ensemble-averaged Gauss equation, namely

$$\langle E_y^+ | y_p^+ \rangle = - \int_{y_p^+}^{Re_\tau} \langle n^* \rangle dy^+, \quad (4)$$

with  $\langle n^* \rangle = \langle n \rangle / n_0 = (2h/N) \int_{-\infty}^{+\infty} f dv_p$  being the dimensionless ensemble-averaged number density. In Eq. (3), the term on the right-hand side represents a collision rate whose particular form is not essential for this discussion, and which is normalized with a characteristic collision time  $t_{coll} = (4/3)(\rho_p/\rho)(t_\nu a_p^+)/\alpha$ , with  $Da = t_\nu/t_{coll}$  being the corresponding collision Damköhler number.

A conservation equation for the wall-normal momentum of the dispersed phase can be obtained by taking the first moment of Eq. (3), or equivalently, by multiplying Eq. (3) by  $v_p$  and integrating in  $v_p$ , which gives

$$St_{ae}^+ \langle (v_p^+)^2 | y_p^+ \rangle \frac{d\langle n^* \rangle}{dy^+} = \underbrace{\langle n^* \rangle \langle v^+ | y_p^+ \rangle}_{\text{Stokes drag}} - \underbrace{St_{ae}^+ \langle n^* \rangle \frac{d}{dy^+} \langle (v_p^+)^2 | y_p^+ \rangle}_{\text{Turbophoretic force}} + \underbrace{St_{el}^{int} \langle n^* \rangle \langle E_y^+ | y_p^+ \rangle}_{\text{Electric force}}, \quad (5)$$

where use of the symmetry condition  $f(y, v_p) = f(y, -v_p)$  has been made along with the relations  $\langle v_p^+ | y_p^+ \rangle = 0$  and  $\langle (v_p^+)^2 | y_p^+ \rangle = \int_{-\infty}^{\infty} v_p^2 f dv_p / \int_{-\infty}^{\infty} f dv_p$ . Note that the relation  $\langle v_p^+ | y_p^+ \rangle = 0$  is required for steady state in terms of mass conservation of the dispersed phase. In contrast,  $\langle v^+ | y_p^+ \rangle \neq 0$  because this quantity is averaged over particle locations at a given distance from the wall and the particles may sample the flow in a biased way. By definition, the collision term in Eq. (3) preserves momentum and therefore does not participate in the momentum balance (5). Note also that a formal solution for the spatial distribution of  $\langle n^* \rangle$  can be straightforwardly obtained by integrating Eq. (5), although the resulting exponential expression is not exploited here since it requires numerical closure of the conditional averages or appropriate approximations studied elsewhere [26, 27].

Equation (5) is convenient for interpreting the concentration profiles in Fig. 2(a) in the following manner. The first two terms on the right-hand side of Eq. (5) correspond, respectively, to the net Stokes drag in the wall-normal direction due to biased sampling of ejection events by inertial particles, and to the turbophoretic force that drives particles toward the wall. In the absence of significant electric effects, the biased sampling of ejection events produces a net drag force away from the wall which counteracts the turbophoresis drift toward the wall. Their balance is responsible for the accumulation of particles in the near-wall region in un electrified turbulent particle-laden flows [26]. In contrast, the last term on the right-hand side of (5) represents the force generated by the self-induced electric field and is strictly negative as observed by the negative sign of the electric field emerging from Eq. (4). This suggests that the collective self-induced electric force drives the particles toward the walls everywhere along the wall-normal direction on average. The magnitude of this force increases from zero at the center of the channel to a value of order  $Re_\tau St_{el}^{int}$  near the wall, where the cumulative effect of all charges above in the channel core becomes important, as prescribed by the Gauss law (i.e., see movie provided in the Supplementary Material [28]). For this reason, the curves in Fig. 2 are labeled according to  $Re_\tau St_{el}^{int}$  instead of just  $St_{el}^{int}$ . For the range of values of  $St_{el}^{int}$  analyzed in this work, the dynamical relevance of the electric force is confined to a near-wall thin layer whose thickness is of the same order as the viscous length  $\delta_\nu$ , whereas the Stokes and turbophoretic forces dominate the motion of the particles throughout the rest of the channel cross section, as shown in Fig. 2(b).

The particles that are aerodynamically entrained in the near-wall thin region mentioned above tend to be held there by the electric field, whose effect is much stronger than the typical flow velocity fluctuations and the ejection events associated with them. In that near-wall region, the electric field participating in Eq. (5) is of order  $Re_\tau \gg 1$ , as indicated by taking the limit  $y^+ \rightarrow 0$  in Eq. (4), and correspondingly, in the first approximation, Eq. (5) simplifies to a balance between the transport of particles by wall-normal velocity fluctuations on the left-hand side and the electric force on the right-hand side. As a result, the relevant parameter that quantifies the internal electric force relative to the aerodynamic force is  $Re_\tau St_{el}^{int}$ , with modest values  $Re_\tau St_{el}^{int} = O(10^{-3})$  already producing significant effects

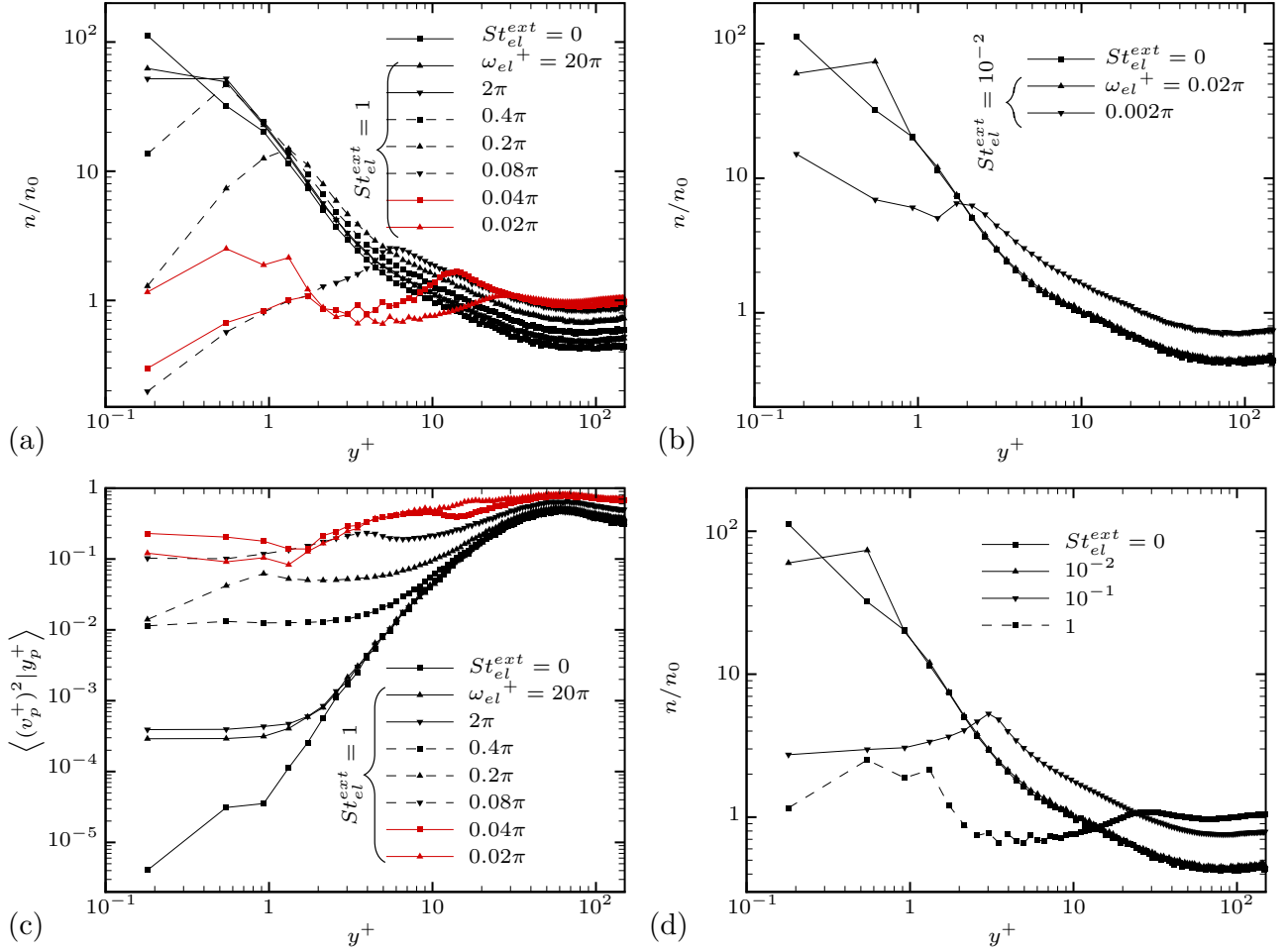


FIG. 3. Dispersed-phase statistics with an applied electric field, including (a) time-averaged number-density profiles in the wall-normal direction for  $St_{el}^{ext} = 1$  while varying  $\omega_{el}^+$ ; (b) time-averaged number-density profiles in the wall-normal direction for  $St_{el}^{ext} = 0.01$  while varying  $\omega_{el}^+$ ; (c) time-averaged variance of the wall-normal particle velocity  $St_{el}^{ext} = 1$  while varying  $\omega_{el}^+$ ; and (d) time-averaged number-density profiles in the wall-normal direction for  $\omega_{el}^+ = 0.02\pi$  while varying  $St_{el}^{ext}$ .

on the concentration profile, as observed in Fig. 2(b). In these conditions, the particles are organized into low-speed streaks of the flow near the wall (not shown here for brevity) despite the prevailing electric force, since the latter acts primarily in the wall-normal direction whereas the streamwise and spanwise velocity fluctuations still determine the horizontal layout of the particles.

### III.2. Collective effects of incident AC electric fields

In this section, the focus is on modifying the near-wall concentration of particles by imposing an oscillating electric field across the channel walls, i.e.,  $|\Delta\Phi_0| > 0$  ( $St_{el}^{ext} > 0$ ) and  $\omega_{el} > 0$  ( $\omega_{el}^+ > 0$ ). All cases described below employ the weakly charged case  $Re_\tau St_{el}^{int} = 1.5 \times 10^{-4}$  and  $St_{el}^{ext} = 0$  as baseline configuration, which displays a turbophoretic behavior not too different from the uncharged case, as observed in Fig. 2(a). Cases with larger values of  $Re_\tau St_{el}^{int}$  require correspondingly larger values of the applied electric field in order to cancel the self-induced electromigration of particles toward the wall described in Sec. III.1.

The suppression of turbophoresis by using AC incident electric fields is first illustrated by the time-averaged concentration profiles shown in Fig. 3(a), which characterizes the effects of varying the oscillation frequency in the range

$0.02\pi \leq \omega_{el}^+ \leq 20\pi$  for  $St_{el}^{ext} = 1$ , with the maximum effect being attained at intermediate values  $\omega_{el}^+ \simeq 0.08\pi$ , for which the resulting number density near the wall is two orders of magnitude smaller than its baseline counterpart value. A similar outcome is achieved even at much weaker electric fields, as observed in Fig. 3(b) for  $St_{el}^{ext} = 0.01$ , although the corresponding near-wall concentration is reduced by just one order of magnitude in this case. The decrease in the number density near the wall is accompanied by a large increase in the variance of the wall-normal particle velocity  $\langle (v_p^+)^2 | y_p^+ \rangle$ , whose profile near the wall becomes increasingly flat as  $\omega_{el}^+$  decreases down to  $\omega_{el}^+ \simeq 0.08\pi$ , below which  $\langle (v_p^+)^2 | y_p^+ \rangle$  decreases following an overall non-monotonic behavior similar to that observed in  $n$ , as shown in Fig. 3(c). Note that  $\langle (v_p^+)^2 | y_p^+ \rangle$  is typically zero or small at the wall in unelectrified flows, whereas here  $\langle (v_p^+)^2 | y_p^+ \rangle$  attains values comparable to  $u_\tau$  because of the prevalence of the electric force near the wall.

Besides the time-averaged results in Fig. 3, additional important information regarding the temporal dynamics of the phenomenon is provided in Fig. 4 in the form of phase averages (indicated by the overbar symbol) over a single voltage-oscillation cycle  $0 \leq \omega_{el}^+ t^+ \leq 2\pi$ . For a given value of  $St_{ae}^+$ , the two relevant parameters that determine the behavior of the solution are  $St_{el}^{ext}$  and  $\omega_{el}^+$ , the latter being the main controlling factor of the temporal dynamics of both the wall-normal particle motion and the near-wall concentration. In principle, increasingly larger values of  $St_{el}^{ext}$  are expected to be increasingly more effective in suppressing turbophoresis, as suggested by the time-averaged results in Fig. 3(d). However, the temporal dynamics emerging from that increase in  $St_{el}^{ext}$ , which is illustrated in Fig. 4 by the change from  $St_{el}^{ext} = 0.1$  in panel (c) to  $St_{el}^{ext} = 1$  in panel (b), indicates that the particles accumulate alternatively on each wall in short-lived intense pockets that lead to long interperiods of very low or zero concentration (i.e., see movie provided in the Supplementary Material [28]). A subsequent increase in  $\omega_{el}^+$ , which is illustrated in Fig. 4 by the change from  $\omega_{el}^+ = 0.02\pi$  in panel (b) to  $\omega_{el}^+ = 0.2\pi$  in panel (d), leads to a less effective suppression of turbophoresis as a result of a delay in the wall-normal particle motion with respect to the oscillating electric field. This delay is a direct consequence of the low-pass filtering nature of the dynamical equilibrium equation for the particles in Eq. (2), in that their motion becomes increasingly insensitive to the electric force as the frequency of the latter increases above the critical value  $1/t_a$  (i.e., for  $\omega_{el}^+ > 1/St_{ae}^+$ ).

The mechanism described above are quantitatively supported by the following argument based on the wall-normal component of the equation of motion of the particles. Consider the Laplace transform of the non-dimensional version of the wall-normal component of second equation in (2), namely

$$\mathcal{L}\{v_p^+\}(s^+) = \frac{1}{1 + St_{ae}^+ s^+} \left[ \mathcal{L}\{v_p^+\}(0^+) + \mathcal{L}\{v^+\}(s^+) + St_{el}^{int} \mathcal{L}\{E_{py}^\infty\}(s^+) + St_{el}^{ext} \frac{s^+}{s^+ + \omega_{el}^+} \right], \quad (6)$$

where  $s^+$  is the dimensionless complex frequency,  $\mathcal{L}\{v_p(s^+)\}$  and  $\mathcal{L}\{v(s^+)\}$  are Laplace transforms of the wall-normal components of the particle velocity and local flow velocity, respectively, and  $\mathcal{L}\{E_{py}^\infty(s^+)\}$  is the Laplace transform of the wall-normal component of the electric field generated by the surrounding charged particles. Note that the last term on the right-hand side of (6) takes into account the effect of the external electric field. Additionally, the prefactor  $(1 + St_{ae}^+ s^+)^{-1}$  in Eq. (6) represents the low-pass filtering character of the response of the particle to an external force. In particular, the cutoff frequency of this filtering process is determined by the particular value of  $St_{ae}^+$  [29].

Equation (6) can be simplified in the following manner. All configurations analyzed in this work consider conditions where  $St_{el}^{ext} \gg St_{el}^{int}$ . For this reason, the contribution of the wall-normal component  $E_{py}^\infty$  of the electric field generated collectively by the particles in (6) can be neglected in the first approximation. Similarly, the second term on the right-hand side of (6) can be neglected if the analysis is restricted to the near-wall region, where the wall-normal fluid velocity is small. With these approximations in mind, and after times of order  $t^+/St_{ae}^+ \gg 1$  have passed such that the transient solution can be neglected, the wall-normal particle velocity obtained from the inverse Laplace transform of Eq. (6) becomes

$$\frac{v_p(t^+)}{u_\tau} = \frac{St_{el}^{ext}}{\sqrt{1 + (St_{ae}^+ \omega_{el}^+)^2}} \cos(\omega_{el}^+ t^+ - \beta). \quad (7)$$

Equation (7) indicates that the wall-normal component of the particle velocity is an oscillatory quantity that has the same frequency  $\omega_{el}$  as the external voltage and a phase delay  $\beta = \arctan(St_{ae}^+ \omega_{el}^+)$ , thereby leading to the formation of time-periodic pockets of particles near the wall, as shown in Fig. 4(b-e). It is noteworthy that the phase delay predicted by this simple description is in good agreement with the phase-averaged velocity fields shown in Fig. 4 (e.g.,  $\beta \sim 17^\circ$  for  $\omega_{el}^+ = 0.02\pi$  and  $\beta \sim 72^\circ$  for  $\omega_{el}^+ = 0.2\pi$ ).

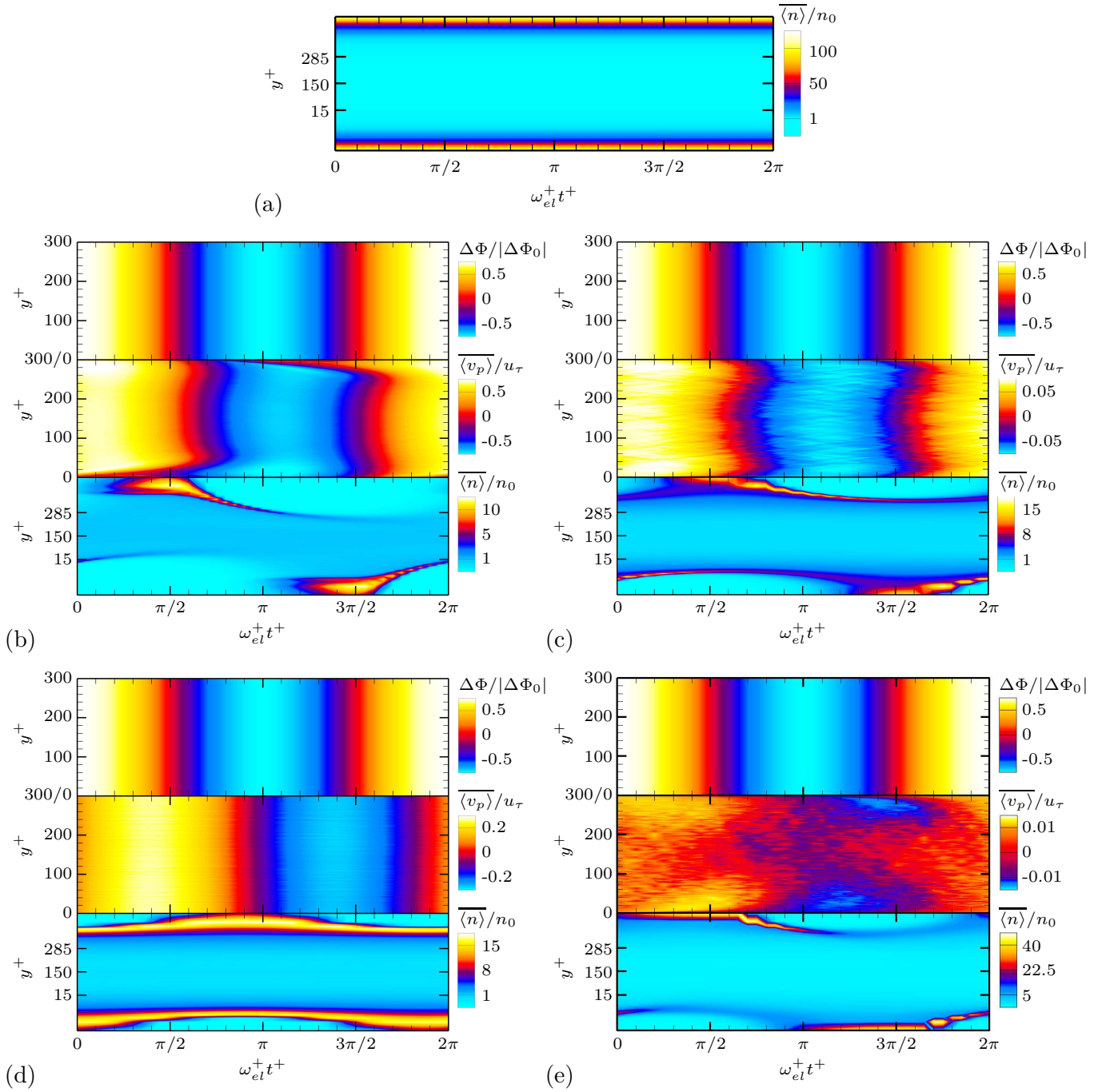


FIG. 4. Dispersed-phase statistics with an applied electric field: (a) Phase-averaged number-density for  $St_{el}^{ext} = 0$ ; The remaining four panels include phase averages of the incident electric field (top subpanel; white, upwards field; light blue, downwards field), wall-normal particle velocity (central subpanel; white, upwards velocity; light blue, downwards velocity), and number density (bottom subpanel, white, high concentration; light blue, low concentration) for (b)  $St_{el}^{ext} = 1$  and  $\omega_{el}^+ = 0.02\pi$ ; (c)  $St_{el}^{ext} = 0.1$  and  $\omega_{el}^+ = 0.02\pi$ ; (d)  $St_{el}^{ext} = 1$  and  $\omega_{el}^+ = 0.2\pi$ ; and (e)  $St_{el}^{ext} = 0.01$  and  $\omega_{el}^+ = 0.002\pi$ .

Based on the above considerations, the non-monotonic variation of the time-averaged near-wall concentration statistics observed in Fig. 3(a) can be therefore explained in the following manner. For order-unity values of  $St_{el}^{ext}$  and  $St_{ae}^+$ , small values of the voltage frequency  $\omega_{el}^+ \ll 1$  necessarily lead to long-lived layers of high concentration of particles on whichever wall is instantaneously charged with a polarity opposite to the charge of the particles, whereas large values  $\omega_{el}^+ \gg 1$  make the wall-normal motion of the particles to lag significantly behind the applied electric field, thereby leading to mostly undisturbed near-wall concentration profiles. The time-averaged maximum suppression of turbophoresis at  $St_{el}^{ext} = 1$  is therefore achieved at an intermediate frequency  $\omega_{el}^+ \simeq 0.08\pi = 1.25/St_{ae}^+$ , as shown in Fig. 3(a).

As commented above, an abatement of turbophoresis can also be achieved with relatively weak incident electric fields, as shown in Fig. 3(b) for  $St_{el}^{ext} = 0.01$ . In this case, both the wall-normal particle velocity and near-wall concentration are almost in phase with the incident electric field, as predicted by Eq. (7) and observed in Fig. 4(d). The resulting wall-normal electromigration flux of particles is confined to the near-wall region, where the incident electric force prevails in a manner that is reminiscent of that shown in Fig. 2(b) for the self-induced electric force. In this way, the electric field is able to just slightly lift the layer of particles from the wall without completely washing them away into the core of the channel as in higher  $St_{el}^{ext}$  cases, which nonetheless proves to be sufficient to decrease the time-averaged near-wall concentration by a factor of 10.

#### IV. CONCLUSIONS

The effects of self-induced and external electric forces on the dynamics of inertial particles in turbulent channel flows have been characterized in this study using DNS in an Eulerian/Lagrangian framework supplemented with appropriate equations for the self-induced and incident electric fields. Two fundamentally different set of cases are treated. In the first set, there is no incident electric field and the particles are transported by turbulence and by the collective self-induced electric forces generated by their own charges. In these conditions, it is found that the suspension of particles behaves similar to an electrical conductor whereby all charges tend to migrate from the core of the channel toward the walls, thereby resulting in an increased near-wall concentration of particles that enhances the turbophoresis effect. In the second set of cases, an incident AC electric field is applied across the channel walls, which leads to suppression of turbophoresis manifested by a decrease in the near-wall concentration of particles by up to two orders of magnitude.

The results presented in this study have been mainly provided in non-dimensional form. It is however illustrative to briefly demonstrate the translation of these results into dimensional figures to address the technical feasibility of the incident electric fields involved. For instance, consider the set of parameters  $St_{ae}^+ = 5$ ,  $a_p^+ = 0.17$ ,  $Re_\tau = 150$ ,  $Re_\tau St_{el}^{int} = 1.5 \cdot 10^{-4}$ ,  $St_{el}^{ext} = 0.1$ , and  $\omega_{el}^+ = 0.02\pi$ , with  $gt_a/u_\tau \ll 1$  and  $\alpha \ll 1$ . The numerical simulations above indicate that these parameters lead to a decrease in the time-averaged near-wall concentration by a factor of 100, as suggested by the simulation results in Fig. 3(d). This set of parameters can be approximately obtained in a channel of half height  $h \simeq 0.01$  m, with air flowing through at friction velocity  $u_\tau \simeq 0.24$  m/s, density  $\rho \simeq 1.2$  kg/m<sup>3</sup>, and kinematic viscosity  $\nu \simeq 1.6 \cdot 10^{-5}$  m<sup>2</sup>/s, and in which solid particles are laden that have a radius  $a_p \simeq 11$   $\mu$ m, number density  $n_0 \simeq 2.5 \cdot 10^8$  m<sup>-3</sup>, material density  $\rho_p \simeq 10^3$  kg/m<sup>3</sup>, and electric charge  $q_p \simeq 14,000|e^-|$ , where  $|e^-|$  is the elementary charge. In this virtual scenario,  $gt_a/u_\tau = O(10^{-2})$  and  $\alpha = O(10^{-3})$ . The amplitude of the required incident electric field would be  $|\Delta\Phi_0|/(2h) \simeq 42$  kV/m with a linear frequency  $\omega_{el}/(2\pi) \simeq 36$  Hz.

In the biperiodic channel flow considered here, the infinite channel width enables the deployment of incident electric fields whose direction is always perpendicular to the two channel walls. However, in practical applications utilizing ducts or pipes, more complex configurations may be required, possibly involving the consideration of rotating electric fields in order to suppress turbophoresis along the entire wall perimeter. Assessments of the electric mechanism of mitigation of turbophoresis proposed here in the presence of other effects of practical interest, including wall roughness, two-way coupling, heat transfer, charge transfer upon collisions, dielectric walls, and gravitational forces, are topics that may be relevant for future research.

#### ACKNOWLEDGMENTS

This investigation was funded by the US DoE/NNSA Grant #DE-NA0002373 as part of the PSAAP-II Center at Stanford, and it was performed during the 2018 CTR Summer Program. The first author is grateful to Prof. Giuseppe

Pascasio for fruitful discussions on this topic.

- 
- [1] M. Caporaloni, F. Tampieri, F. Trombetti, and O. Vittori, “Transfer of Particles in Nonisotropic Air Turbulence,” *Journal of the Atmospheric Sciences* **32**, 565–568 (1975).
  - [2] M. Reeks, “The transport of discrete particles in inhomogeneous turbulence,” *Journal of Aerosol Science* **14**, 729–739 (1983).
  - [3] B. Milici, M. De Marchis, G. Sardina, and E. Napoli, “Effects of roughness on particle dynamics in turbulent channel flows: A DNS analysis,” *Journal of Fluid Mechanics* **739**, 465–478 (2014).
  - [4] W. John, G. Reischl, and W. Devor, “Charge transfer to metal surfaces from bouncing aerosol particles,” *Journal of Aerosol Science* **11**, 115–138 (1980).
  - [5] P. Kolniak and R. Kuczynski, “Numerical modeling of powder electrification in pneumatic transport,” *Journal of Electrostatics* **23**, 421–430 (1989).
  - [6] S. Matsusaka, H. Umemoto, M. Nishitani, and H. Masuda, “Electrostatic charge distribution of particles in gas-solids pipe flow,” *Journal of Electrostatics* **55**, 81–96 (2002).
  - [7] S. Matsusaka, H. Maruyama, T. Matsuyama, and M. Ghadiri, “Triboelectric charging of powders: A review,” *Chemical Engineering Science* **65**, 5781–5807 (2010).
  - [8] H. Grosshans and M. V. Papalexandris, “Large Eddy simulation of triboelectric charging in pneumatic powder transport,” *Powder Technology* **301**, 1008–1015 (2016).
  - [9] A. U. Karnik and J. S. Shrimpton, “Mitigation of preferential concentration of small inertial particles in stationary isotropic turbulence using electrical and gravitational body forces,” *Physics of Fluids* **24**, 0–16 (2012).
  - [10] J. Lu and R. A. Shaw, “Charged particle dynamics in turbulence: Theory and direct numerical simulations,” *Physics of Fluids* **27**, 065111 (2015).
  - [11] H. Grosshans and M. V. Papalexandris, “Direct numerical simulation of triboelectric charging in particle-laden turbulent channel flows,” *Journal of Fluid Mechanics* **818**, 465–491 (2017).
  - [12] H. Grosshans, “Modulation of particle dynamics in dilute duct flows by electrostatic charges,” *Physics of Fluids* **30**, 083303 (2018).
  - [13] Y. Yao and J. Capecelatro, “Competition between drag and Coulomb interactions in turbulent particle-laden flows using a coupled-fluidEwald-summation based approach,” *Physical Review Fluids* **3**, 034301 (2018).
  - [14] M. Di Renzo and J. Urzay, “Aerodynamic generation of electric fields in turbulence laden with charged inertial particles,” *Nature Communications* **9**, 1676 (2018).
  - [15] C. Marchioli, A. Soldati, J. G. M. Kuerten, B. Arcen, A. Tanière, G. Goldensohn, K. D. Squires, M. F. Cargnelutti, and L. M. Portela, “Statistics of particle dispersion in direct numerical simulations of wall-bounded turbulence: Results of an international collaborative benchmark test,” *International Journal of Multiphase Flow* **34**, 879–893 (2008).
  - [16] Q. Wang, K. D. Squires, M. Chen, and J. B. McLaughlin, “On the role of the lift force in turbulence simulations of particle deposition,” *International Journal of Multiphase Flow* **23**, 749–763 (1997).
  - [17] J. Young and A. Leeming, “A theory of particle deposition in turbulent pipe flow,” *Journal of Fluid Mechanics* **340**, 129–159 (1997).
  - [18] P. Costa, L. Brandt, and F. Picano, “Interface-resolved simulations of small inertial particles in turbulent channel flow,” arXiv preprint arXiv:1906.01249 (2020).
  - [19] Y. Li, J. B. McLaughlin, K. Kontomaris, and L. Portela, “Numerical simulation of particle-laden turbulent channel flow,” *Physics of Fluids* **13**, 2957–2967 (2001).
  - [20] Y. Yamamoto, M. Potthoff, T. Tanaka, T. Kajishima, and Y. Tsuji, “Large-eddy simulation of turbulent gas-particle flow in a vertical channel: Effect of considering inter-particle collisions,” *Journal of Fluid Mechanics* **442**, 303–334 (2001).
  - [21] N. Caraman, J. Borée, and O. Simonin, “Effect of collisions on the dispersed phase fluctuation in a dilute tube flow: Experimental and theoretical analysis,” *Physics of Fluids* **15**, 3602–3612 (2003).
  - [22] J. G. Kuerten and A. W. Vreman, “Effect of droplet interaction on droplet-laden turbulent channel flow,” *Physics of Fluids* **27** (2015), 10.1063/1.4921492.
  - [23] L. Greengard and V. Rokhlin, “A fast algorithm for particle simulations,” *Journal of Computational Physics* **73**, 325–348 (1987).
  - [24] M. Esmaily, L. Jofre, A. Mani, and G. Iaccarino, “A scalable geometric multigrid solver for nonsymmetric elliptic systems with application to variable-density flows,” *Journal of Computational Physics* **357**, 142–158 (2018).
  - [25] F. A. Williams, “Spray combustion and atomization,” *Physics of Fluids* **1**, 541–545 (1958).
  - [26] P. L. Johnson, “Toward wall-modeled LES of particle-laden flows : Analysis of turbophoresis and inter-particle collisions in a turbulent channel flow,” Center for Turbulence Research, Annual Research Briefs , 111–124 (2018).
  - [27] P. L. Johnson, M. Bassenne, and P. Moin, “Turbophoresis of small inertial particles: theoretical considerations and application to wall-modelled large-eddy simulations,” *Journal of Fluid Mechanics* (in press) (2020).
  - [28] See Supplemental Material at <http://www.myurl.com> for “Visualization of the computed motion of: electrically uncharged particles; electrically charged particles without an external electric field; electrically charged particles with an external

electric field”.

- [29] J. Urzay, M. Bassenne, G. I. Park, and P. Moin, “Characteristic regimes of subgrid-scale coupling in LES of particle-laden turbulent flows,” Center for Turbulence Research Annual Research Briefs , 3–13 (2014).